Pumped thermal energy storage systems integrated with a concentrating solar power section: conceptual design and performance evaluation

Mario Petrollese*, Mario Cascetta, Vittorio Tola, Daniele Cocco and Giorgio Cau
Department of Mechanical, Chemical and Materials Engineering, University of Cagliari, Via Marengo, 2 09123 Cagliari, Italy
* Corresponding Author: Mario Petrollese
petrollese@unica.it, Tel. ++39 070 6755118

Abstract

A novel Pumped Thermal Energy Storage (PTES) system thermally integrated with a Concentrating Solar Power (CSP) plant is proposed and investigated. The two sections operate with the same working fluid, share several components and can operate simultaneously or independently of each other. A Thermal Energy Storage (TES) system composed of three thermocline packed-bed tanks is included. Specific mathematical models were developed to simulate the performance of the integrated PTES-CSP plant under nominal conditions and to evaluate the thermal profiles of the TES tanks. As a case study, an integrated PTES-CSP system characterized by a nominal power of 5 MW with a nominal storage capacity of 4 equivalent hours was considered. The influence of the main design parameters, namely the pressure ratio and the operating temperatures of the TES system, on the main performance indices was investigated. The results demonstrated that the exergetic roundtrip efficiency of the integrated plant reaches a maximum for a pressure ratio of about 5.2. A sensitivity analysis on the solar receiver temperature and turbomachinery polytropic efficiency and maximum allowable temperatures was also conducted. Finally, a feasible design for the PTES-CSP system characterized by an exergetic roundtrip efficiency of about 60% was proposed.

Keywords:

Energy Storage; Concentrating Solar Power; Pumped Thermal Energy Storage; Packed Bed Thermal Energy Storage.

NOMENCLATURE

Symbols

A	area [m^2]
c	specific heat [kJ/kg K]
d	diameter [m]
e	specific exergy [kJ/kg]
h	specific enthalpy [kJ/kg]
$\dot{m}$	mass flow rate [kg/s]
k	thermal conductivity [W/m K]
s	specific entropy [kJ/kg K]
t	time [h]
T	temperature [K]
V	volume [m^3]
$\dot{W}$	electrical power [kW]
α	heat transfer coefficient [W/m^2 K]
β	pressure ratio
γ	power ratio
ε	void fraction
η	efficiency
ρ	density [kg/m^3]

Subscripts

C	compressor
S	solid medium
T	turbine
WF	working fluid

Acronyms

CAES	Compressed Air Energy Storage
CSP	Concentrating Solar Power
PHES	Pumped Hydroelectric Storage
PTES	Pumped Thermal Energy Storage
RES	Renewable Energy Source
TES	Thermal Energy Storage
TSO	Transmission System Operator
WCO	Water cooler

1. Introduction

Nowadays, the transition toward a decarbonized and sustainable energy sector by means of a strong penetration of Renewable Energy Sources (RES) in the energy mix is considered a non-postponable process for tackling climate change. However, the variable and unpredictable nature of RES – solar and wind in particular – demands the deployment of several actions for matching the supply and demand of energy at various grid levels [1]. Among them, the implementation of utility-scale energy storage systems is assuming a vital importance to allow the separation of energy production from its consumption, to compensate for power fluctuations and to provide a more regular and predictable power profile. This service requires high storage capacities at relatively low cost [2]. Among utility-scale energy storage systems, Pumped Hydroelectric Storage (PHES) is currently the most cost-effective technology for storing large amounts of electrical energy [3]. However, the need for suitable geographical locations limits its diffusion. Moreover, the environmental impact is also not negligible in terms of land occupation, disturbance of aquatic life and changes in the natural water flows. Compressed Air Energy Storage (CAES) is another interesting option for medium- and large-scale energy storage, potentially more cost-effective than batteries and with less environmental impact compared to PHES. On the other hand, the use of natural geological formations, like salt mines fallen into disuse, often proposed to limit the initial costs, reduces the storage pressure and thus its energy density.

Furthermore, the pressure changes continuously during charge and discharge, leading to a continuous off-design operation of the compressors/turbines, which reduces the overall plant efficiency [4]. Consequently, the increase of non-dispatchable RES capacity and the consequent requirement for large storage capacities cannot be fully covered only by PHES systems and so alternative technologies for medium- and large-scale energy storage need to be investigated [5].

Pumped Thermal Energy Storage (PTES) is a promising electrical energy storage technology characterized by high energy density, high roundtrip efficiency and no requirement for special sites for its installation [6]. PTES systems are constituted by a power block that can operate both as a heat pump and a heat engine and a Thermal Energy Storage (TES) system including low-temperature (LT) and high-temperature (HT) reservoirs. During the charging process, electricity is used to pump heat from the LT reservoir to the HT reservoir through a reverse power cycle. Conversely, during the discharging process, the stored thermal energy is converted into electricity through a power cycle. In recent years, various PTES systems have been proposed based on different thermodynamic cycles, such as Rankine and Brayton-Joule [7]. Among them, the research on Brayton-based PTES is currently the most advanced, proposing studies on various plant configurations, in-depth analyses of their thermodynamic aspects and on performance evaluation under different operating conditions [8]. In this regard, the effect on the main performance indices of the design solutions, such as maximum and minimum cycle temperatures and pressure ratios, was investigated by Guo et al. [9], who found the optimal configuration of a Brayton-based PTES system. However, as highlighted by McTigue et al. [10], the achieved performance in terms of roundtrip efficiency is highly sensitive to the losses occurring in compression and expansion processes. This was confirmed by the exergy analysis conducted by Zhao et al. [11], indicating the maximum exergy destruction rate in the expander during the discharging phase. Advanced exergy analysis further revealed that, among the system components studied, the cold heat exchanger during discharge is associated with the largest share (95%) of the avoidable exergy destruction rate. The thermodynamics and heat transfer process affecting PTES performance were also investigated by Wang et al. [12], who highlighted the importance of the main design parameters of TES systems, such as particle size, aspect ratio, etc., in achieving the maximum roundtrip efficiency and a suitable discharging power stability. In this regard, Wang at al. [13] investigated PTES performance considering different TES arrangements in terms of the number of reservoirs and operating modes. The results demonstrated that the operating modes strongly influence the roundtrip efficiency of the system and the delivery power variation ratio, while the number of reservoirs has a minor impact on the performance. In all the previous papers, the TES section is based on sensible packed-bed heat storage systems, while the most common working fluid is argon. However, other working fluids, such as air, carbon dioxide, helium, etc., have been studied [14]. As stated by Dumont et al. [15], roundtrip efficiencies of about 60–70% are often claimed in the literature, but these values are achieved with very high compressor/turbine polytropic efficiencies (over 90%). Since the latter have a considerable impact on the efficiency of a Brayton-PTES system, a strong reduction in roundtrip efficiency would be expected if slightly lower polytropic efficiencies were assumed.

For this reason, innovative solutions should be investigated for making such storage systems competitive with other storage technologies. An alternative PTES configuration was proposed by Benato [16], in which an electrical heater is included after the compressor to convert electrical energy into thermal energy, aiming to make the maximum cycle temperature independent of the compressor pressure ratio. Although the presence of the electrical heater reduces the roundtrip efficiency, the author demonstrated that a decrease in heat exchange areas and compressor size, and thus in PTES specific costs, is expected. The potentiality of a PTES as a combined cooling, heating and power system was investigated by Zhang et al. [17]. Their results demonstrated that actively and appropriately delivering heat from the hot reservoir can improve the stability of the outlet temperature of the working fluid during the discharging phase, thereby improving the electrical efficiency and power delivery stability of the system. As stated by Dumont et al. [15], thermal integration with other systems could lead to substantial advantages in terms of reduction of electricity losses. In this regard, the effect of integrating external heat sources and/or heat sinks in a PTES system was investigated by Jockenhofer et al. [18] who demonstrated the benefits in terms of increasing the roundtrip efficiency and exergy efficiency. The possible combination of a PTES with a natural gas distribution system using LNG cold energy as a heat sink was proposed and analysed by Wang et al. [19], who confirmed the feasibility of thermal integration and the potential improvement in roundtrip efficiency.

Brayton cycle PTES systems could also be suitably integrated with Concentrating Solar Power (CSP) plants. CSP is an effective technology for converting solar energy into electricity, but the intermittent nature of solar radiation limits the capacity factors achievable by these systems. The integration of CSP plants with PTES systems is a possible solution to overcome this limitation. Moreover, the possible sharing of some components between the two sections (such as the power generation section and the TES system) would lead to significant savings in capital costs [20]. Although the integration of PTES systems with CSP plants could lead to various potential benefits, only the study recently proposed by McTigue et al. [21] has investigated this possibility. In particular, the paper explored the combination of PTES with a CSP plant using an sCO_2 power block with a second recompression at temperatures higher than the maximum one reached in the heat pump cycle. The results demonstrated the feasibility of integrating a PTES system with a solar source, but the proposed scheme, which does not include any additional TES system for the solar section, produces slightly less electricity per unit of solar heat input over a charge–discharge cycle than a stand-alone CSP cycle.

Consequently, to effectively integrate a PTES system with a solar-based power plant, the real technical potential for an integrated PTES-CSP systems needs to be investigated in more depth. For this reason, a novel integrated PTES-CSP plant is proposed in this study A simulation model has been developed in the MATLAB environment to evaluate the performance of the single sections and of the overall system. In particular, the performance of the integrated system is evaluated as a function of the main design parameters: the compressor pressure ratio and the outlet temperatures of the water coolers. Since the integrated system is fed by two different energy sources, namely, electrical energy from the grid and thermal energy from the solar receiver, its performance has been assessed by using exergy performance indices. In particular, the nominal exergy roundtrip efficiency of both the integrated PTES-CSP and the PTES systems, as well as the exergy efficiency

of the CSP section and the ratio of the power produced by the PTES section to that produced by the integrated PTES–CSP system during their discharging phases, have been calculated and discussed. Moreover, as a case study, an integrated PTES–CSP system using argon as the working fluid, a nominal power of 5 MW and a storage capacity of 4 equivalent hours of operation at design conditions has been considered. The preliminary design for this case study, in terms of the volume, diameter and height of the storage vessels, as well as the size of compressors and turbines, has been carried out. Moreover, a sensitivity analysis has been carried out on the polytropic efficiency of the compressor and turbine and on their maximum temperature.

2. System configuration

As mentioned in the previous section, a PTES system is a storage system in which the electrical energy is used to store thermal energy in hot and cold reservoirs during the charging phase, which is reconverted into electricity during the discharging phase. Figure 1 shows the scheme of a typical PTES system based on a Brayton cycle and the corresponding thermodynamic cycles for both the charging and discharging phases. In addition to the hot and cold reservoirs, the system is equipped with two compressors (C1 and C2), two turbines (T1 and T2), an electric motor/generator (M/G) and two water coolers (WCO1 and WCO2). The system operates as a Brayton heat pump during the charging phase: the working fluid is compressed by C1 (10–11), reaching the maximum cycle pressure and temperature, and subsequently sent to the hot reservoir for charging this TES system (11–12). A further cooling (12–13) is performed in WCO1 to allow the working fluid to close the thermodynamic cycle, overcoming the turbomachinery irreversibilities. The following expansion in T1 (13–14) leads to temperatures usually lower than the ambient one. Therefore, the working fluid is taken back to the initial conditions (14–9) and the cryogenic energy is stored in the cold reservoir. Since the work of the cycle is negative, the required power is supplied by the electrical grid.

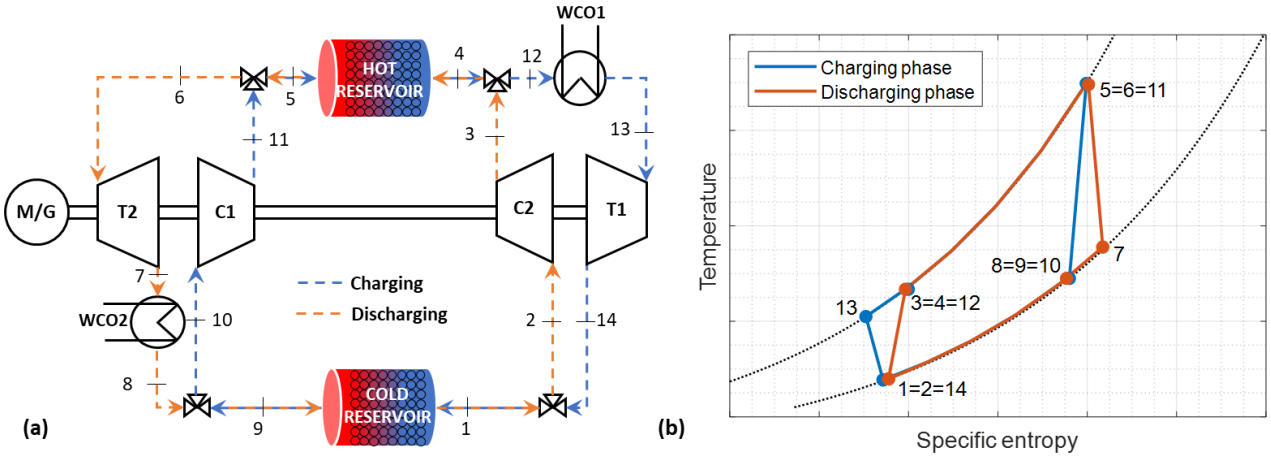

Figure 1 – (a) Schematic of a typical Brayton-based PTES system and (b) thermodynamic cycles in the temperature–entropy diagram.

During the discharging phase, the system operates as a Brayton heat engine: the working fluid is cooled down to minimum cycle temperature in the cold reservoir (9-2), compressed by C2 (2–3), then, it is heated up in the hot reservoir (3–5), reaching the maximum cycle temperature, and subsequently it expands in T2 (5–7). A second water cooler (WCO2) reduces the temperature of the working fluid (7–8) to the initial conditions. In this operating condition, the work of the cycle is positive and the ratio of the electrical energy produced during the discharging phase to that absorbed during the charging phase defines the roundtrip efficiency of the PTES system. As shown in Figure 1(b), in a PTES system the maximum temperature (T_{11}, which is also equal to T_5 and T_6) directly depends on the compressor pressure ratio and, therefore, an increase of this design parameter could be beneficial for the performance of the storage system. On the other hand, several issues may arise with high values of the pressure ratio: (i) the maximum cycle temperature corresponds with the outlet temperature of the last compressor stage and currently there are few compressor technologies able to handle temperatures higher than 800–850 K; (ii) the design of the hot reservoir could be demanding, due to the high operating pressures; (iii) the variation of temperature profiles inside the packed-bed TES system leads to corresponding variations of the turbomachinery inlet temperatures and therefore of the minimum/maximum cycle temperatures. The introduction of an external HT thermal input could partially overcome the above-mentioned critical issues. For this reason, the integration of a PTES system with a CSP plant is proposed and investigated in this study.

The configuration of the integrated PTES–CSP system here considered is shown in Figure 2. The two sections (PTES and CSP) operate with the same working fluid, share several components and can operate simultaneously or independently of each other.

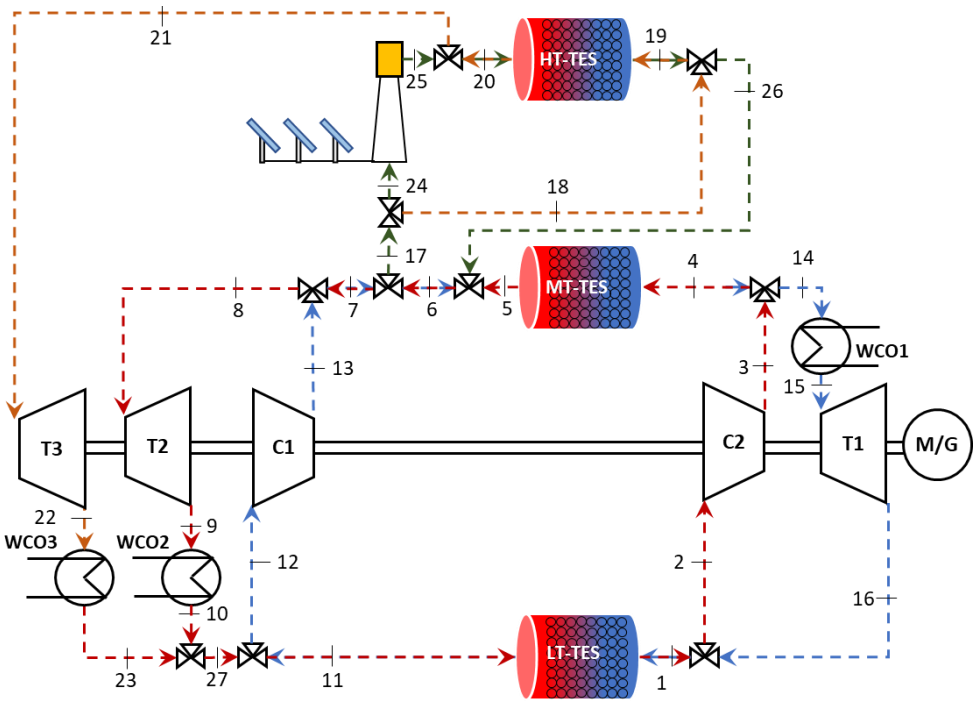

Figure 2 – System configuration of the integrated PTES–CSP plant.

Compared to the solely PTES configuration, a gas-phase solar receiver is included together with an additional high-temperature reservoir (HT-TES), a turbine (T3) and a water cooler (WCO3). Since PTES systems usually operate with limited pressure ratios to avoid too high a pressure in the hot reservoir, direct heating of the working fluid in the receiver is a viable choice, avoiding the use of a gas-to-gas heat exchanger or high costs for piping, receiver and vessel due to high pressures. Overall, the integrated plant is composed of three TES systems to deal with the intermittent nature of solar radiation and to give the flexibility required by an electrical energy storage system devoted to providing ancillary services to the grid. As shown by Figure 2, the integrated system includes an HT-TES for dealing with the intermittence of solar energy availability and increasing the capacity factor of the CSP section, a medium temperature TES (MT-TES) and a low temperature TES (LT-TES), corresponding to the hot and cold reservoirs of the PTES system in Figure 1. The gaseous nature of the working fluid leads to the choice of a single-tank thermocline packed-bed system for all three TES sections.

For a better understanding of the behaviour of the integrated system, Figure 3 and Figure 4 show the system configuration and the corresponding thermodynamic cycle during the charging and discharging phases, respectively. The first operating mode (charging) occurs during periods of electrical energy overproduction and simultaneous availability of thermal power from the solar receiver. In these conditions, the delivery of power from the CSP section is not convenient for either the plant owner, since the selling prices are usually low in these conditions, or the Transmission System Operator (TSO), since it would further affect the grid power balance. For this reason, this operating mode is used only to charge the HT-TES with the thermal energy available from the solar source while the net energy absorbed from the grid (that is, the difference between the energy required by the compressor and that produced by the turbine) is used to 'pump' heat from the LT-TES to the HT-TES and MT-TES. As shown in Figure 3(a), after compression in C1 (1C–2C), the working fluid reaches its maximum temperature in the receiver (2C–3C). Subsequently, it is sent to the HT-TES to store the thermal power obtained from the solar source (3C–4C). This storage section is arranged to obtain a working fluid outlet temperature equal to that set as the maximum inlet temperature of the MT-TES.

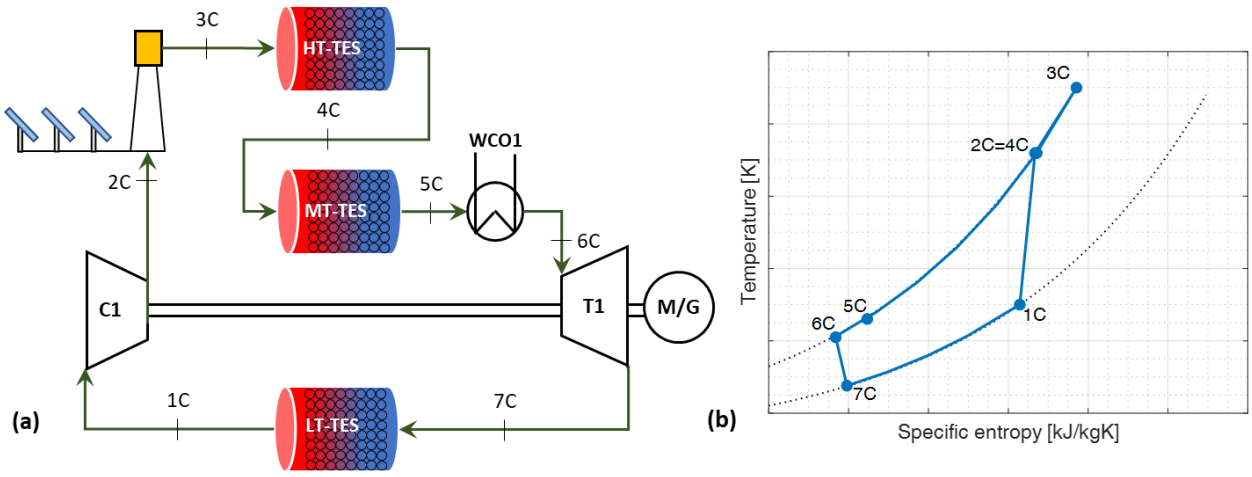

Figure 3 – (a) Schematic of the integrated PTES–CSP plant during charging mode and (b) corresponding thermodynamic cycle.

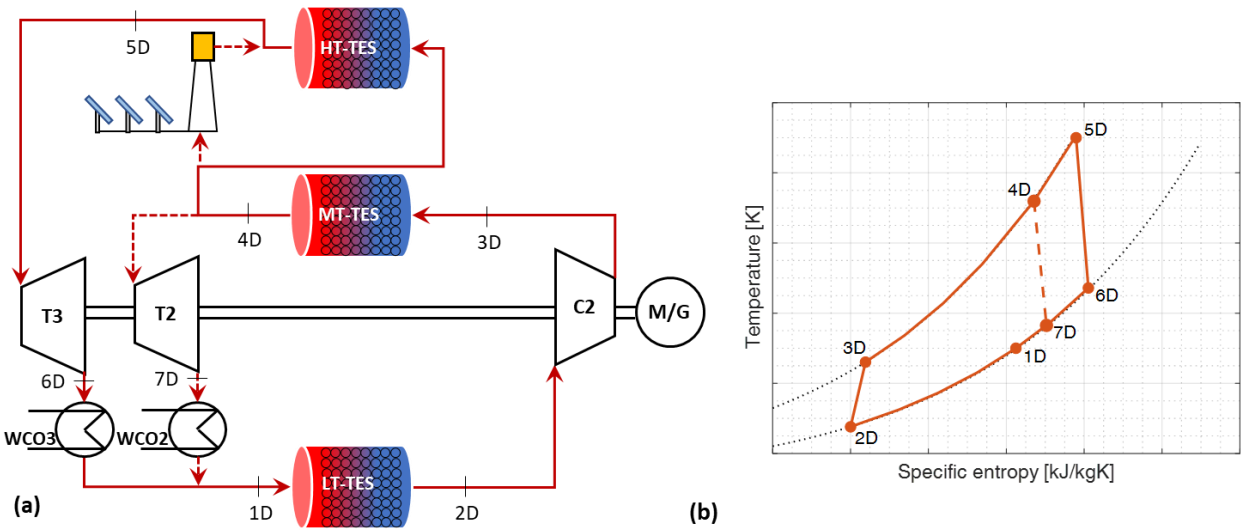

Figure 4 – (a) Schematic of the integrated PTES–CSP plant during discharging mode and (b) corresponding thermodynamic cycle.

The working fluid then follows the same path as for the PTES-only charging phase: a first cooling in the MT-TES, a further cooling in the WCO1 up to a designed temperature, an expansion in T1 and a heating in the LT-TES.

As can be seen, in the PTES–CSP configuration the maximum temperature of the PTES section (T_{4C}) does not directly depend on the compressor outlet temperature, unlike in the PTES-only system, but on the minimum temperature in the HT-TES, which is usually more stable and less sensitive to variation of operating conditions. Furthermore, the receiver would operate at low pressures (as mentioned, the pressure ratio in a PTES system is generally below 10), but with high inlet temperatures (required to assure proper performance when the system operates in PTES-only mode). This could be beneficial both from an energetic point of view, since the irreversibility would be minimized, and from an economic point of view, with an easier design of the receiver. During the discharging phase of the integrated PTES–CSP plant, the energy stored in the three TES systems is used to produce electrical energy. As can be observed in Figure 4(a), the working fluid is cooled down to reach the minimum temperature of the LT-TES (1D–2D) before entering the compressor C2 (2D–3D). An important increase of the working fluid temperature then occurs thanks to the energy stored in the MT-TES (3D–4D) and the HT-TES (4D–5D), together with the energy eventually produced by the solar field. Downstream of the heating process, the working fluid expands in turbine T3 (5D–6D) and it is subsequently cooled in WCO3 (6D–1D) to reach the initial temperature. The thermal energy released by the working fluid in this cooler is usually characterized by a relative high energy quality and therefore it can be available for external use. Finally, it is worth noting that the proposed system configuration could also operate in CSP-only mode. As shown in Figure 5(a), in this operating mode, the compressor C1 is used to increase the pressure of the working fluid (1S–2S). After a further increase of the temperature by means of the solar receiver and/or the HT-TES (2S–3S), the working fluid expands in turbine T3 (3S–4S) and then is cooled by WCO3 (4S–1S). However, it is expected that this operating mode would be used infrequently, due to both the intermittent availability of the solar source and the probable continuous request for ancillary services by the TSO.

Obviously, as better discussed below, the system can also operate in PTES-only mode by following the charging and discharging cycles in Figure 1(b).

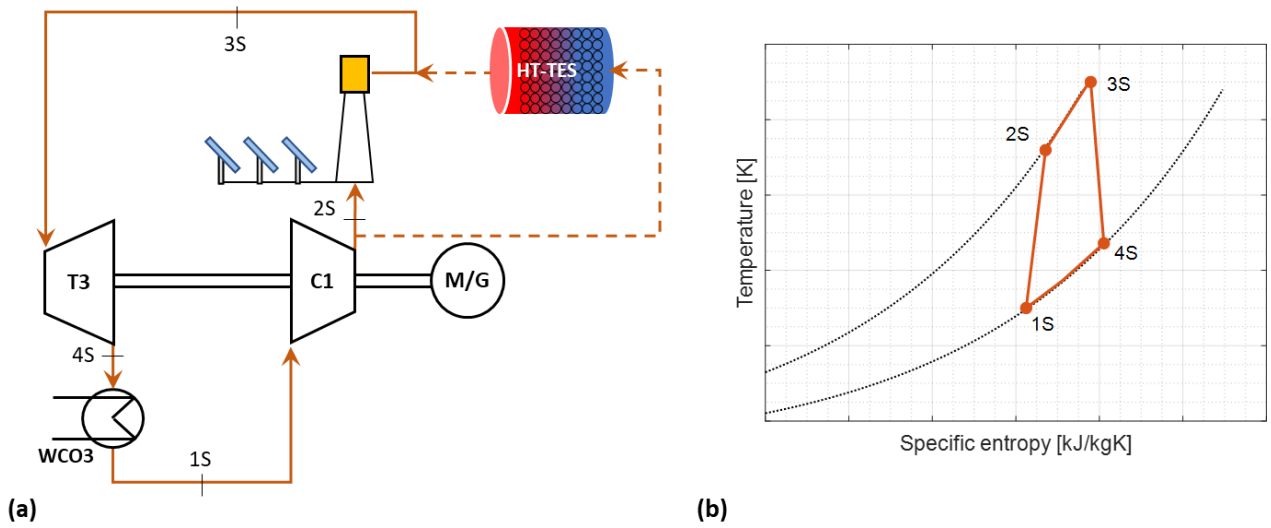

Figure 5 – (a) Schematic of the integrated PTES–CSP plant during CSP-only operating mode and (b) corresponding thermodynamic cycle.

3. Methods

The main assumptions and the mathematical models used for assessing the performance of the integrated PTES–CSP plant are introduced in this section. First, the method used for determining the thermodynamic cycles during design conditions is presented. Subsequently, the sizing of the main components, in particular of the three TES systems, is introduced. Finally, the performance indices adopted for evaluating the various sections and the overall system are defined. All the mathematical models were implemented in the MATLAB environment, while the Coolprop database [10] was used for the evaluation of working fluid properties.

3.1. Thermodynamic cycles

The first step concerns the definition of the reference thermodynamic cycles followed by the integrated PTES–CSP plant during the various operating phases. It is assumed that under design conditions the inlet and outlet temperatures of the three TES systems are univocal. Consequently, to achieve a univocal LT-TES maximum temperature regardless of the discharging mode adopted (PTES-only or PTES–CSP), the working fluid temperatures at the outlet side of WCO3 and WCO2 are the same. Furthermore, the minimum temperature of the HT-TES is equal to the compressor outlet temperature to achieve the same MT-TES maximum temperature during the charging phase of both the PTES-only and the integrated PTES–CSP operating phases.

Three design variables are identified for determining all the thermodynamic states: the compressor pressure ratio (β_C), the WCO1 outlet temperature (T_{WCO1}) and the WCO2 outlet temperature (T_{WCO2}). The latter is also equal to the WCO3 outlet temperature. For each variable, a range of feasible values is assumed to define the search space of the potential reference cycles, as reported in Table 1.

A minimum cycle pressure of 1 bar is set as the design value, but lower pressures could be imposed in the closed-loop Brayton cycle to limit the maximum pressure operating in the receiver and HT-TES and MT-TES by keeping the same pressure ratio. A maximum temperature of 1000 K can be considered as an achievable target for a gas receiver, regardless of the receiver architecture [22]. According to McTigue et al. [10,12], argon is chosen as the working fluid thanks to the high ratio of the specific heat at constant pressure to that at constant volume, while the polytropic efficiency of the turbines and compressors is set to 0.90. A relative pressure loss of 2% in the three TES systems, in the receiver and in the three water coolers is also assumed. Finally, two constraints are imposed concerning the minimum and maximum temperatures in the compressors and turbines. In accordance with White et al. [7,16], these temperatures are set considering the current technological limitations in compressor design. All the design parameters and assumptions are summarized in Table 1.

Table 1 – Main parameter assumptions and variable ranges set for determining the design of the thermodynamic states of the integrated PTES–CSP plant.

Parameter	**Value**	**Variable**	**Range**
Minimum cycle pressure	1 bar	Compressor pressure ratio	2–7
Outlet receiver temperature	1000 K	Outlet WCO1 temperature	310–600 K
Working fluid	Argon	Outlet WCO2/WCO3 temperature	310–600 K
Turbine polytropic efficiency	0.90	**Constraints**	**Value**
Compressor polytropic efficiency	0.90	Turbomachinery minimum temperature	173 K
Relative pressure losses	2%	Turbomachinery maximum temperature	823 K

Once the thermodynamic cycle is defined, the specific exergy (e) of all the streams is determined and then used for the performance evaluation. Since a closed-loop cycle with the same working substance has been studied, only the physical component of specific exergy is considered:

$$e = (h - h_0) - T_0(s - s_0) \quad (1)$$

where h and s are the specific enthalpy and entropy of the stream, respectively, T_0 is the reference temperature (assumed to be 298.15 K), and h_0 and s_0 are the reference specific enthalpy and entropy, respectively (a reference pressure of 1.013 bar is set).

3.2. Sizing of the main plant components

For a given thermodynamic cycle, sizing of the main components is carried out by means of two design parameters: the net power produced by the integrated PTES–CSP plant during the discharging phase under design conditions ($\dot{W}_{PTES-CSP,D}$) and the nominal storage capacity of the TES section (Δt_{TES}), expressed in terms of equivalent hours of operation of the plant under nominal conditions.

In particular, the mass flow rate of the working fluid ($\dot{m}_{WF}$) is calculated in accordance with the useful power produced by the integrated plant during the discharging phase, as:

$$\dot{m}_{WF} = \frac{\dot{W}_{PTES-CSP,D}}{[(h_{5D} - h_{6D}) - (h_{3D} - h_{2D})]} \quad (2)$$

The compressor C1, the turbine T1 and the water cooler WCO1 are designed in accordance with the thermodynamic states during the charging phase, while compressor C2, turbines T2 and T3, and water coolers WCO2 and WCO3 are sized considering the operating temperatures and pressure during the design discharging phase. Moreover, the study focuses on cycle assessment and therefore mechanical losses, auxiliary consumption and solar field efficiency are neglected.

3.2.1. TES sizing and modelling

As stated previously, the plant includes a TES system based on three thermocline packed-bed tanks at different temperature levels, each sized to provide the required storage capacity Δt_{TES}. Granite pebbles are chosen as the solid storage medium for their low cost and because they can suitably bear the extreme temperatures reached by the working fluid. The stored energy (E_{TES}) can be therefore calculated as:

$$E_{TES} = \dot{m}_{WF}\bar{c}_{WF}(T_{WF,max} - T_{WF.min}) \cdot \Delta t_{TES} \quad (3)$$

where $\bar{c}_{WF}$ is the average specific heat of the working fluid, while $T_{WF,max}$ and $T_{WF.min}$ are the maximum and minimum fluid temperatures inside the TES system, respectively. Starting from the amount of energy stored, the theoretical tank volume ($V_{TES,t}$), namely, the storage volume required if the entire packed bed is heated up from the minimum temperature ($T_{WF,min}$) to the maximum temperature ($T_{WF,max}$), is calculated as follows:

$$V_{TES,t} = \frac{E_{TES}}{(\bar{\rho}_S\bar{c}_S(1-\varepsilon) + \bar{\rho}_{WF}\bar{c}_{WF}\varepsilon) \cdot (T_{WF,max} - T_{WF.min})} \quad (4)$$

where $\bar{\rho}_S$ is the average density of the solid medium (assumed equal to 2688 kg/m^3), $\bar{\rho}_{WF}$ is the average density of the working fluid, $\bar{c}_S$ is the specific heat of the solid medium and ε is the void fraction of the bed, here assumed to be 0.4. Since the packed bed should operate in a wide temperature range (from below 273 K up to 1000 K), empirical correlations obtained from experimental tests [23,24] are used for evaluating the main thermal properties of the solid medium, as shown in Figure 6.

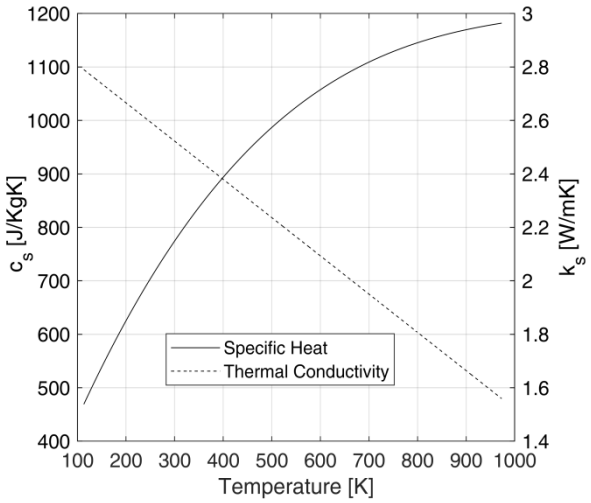

Figure 6 – Specific heat and thermal conductivity of the granite pebbles against temperature.

A transient 1-D two-equation model was implemented for simulating the thermal behaviour of the TES system, required for determining the actual tank volume. By assuming a homogeneous and isotropic bed with a constant radial temperature profile, the temperature profiles along the bed for both the working fluid (T_{WF}) and the solid medium (T_S) are calculated by means of the following equations:

$$\varepsilon\rho_{WF}c_{WF}\frac{\partial T_{WF}}{\partial t}+\rho_{WF}c_{WF}u\frac{\partial T_{WF}}{\partial z}=\alpha_c A_S(T_S-T_{WF})-U_{TES}A_{TES}(\overline{T}_{WF}-T_{AMB}) \quad (5)$$

$$(1-\varepsilon)\rho_S c_S\frac{\partial T_S}{\partial t}=k_{eff}\frac{\partial^2 T_S}{\partial z^2}+\alpha_c A_S(T_{WF}-T_{BED}) \quad (6)$$

where k_{eff} is the effective thermal conductivity that also takes into account the radiation contribution [25] within the bed. A_S and α_c are the superficial area per unit of volume of the bed and the convective heat transfer coefficient, respectively, U_{TES} is the overall heat transfer coefficient between the tank and the environment (set to 0.3 W/m^2 K), A_{TES} is the superficial area per unit of volume of the vessel and T_{AMB} is the ambient temperature.

The convective heat transfer coefficient α is strictly dependent on the Nusselt number evaluated using the well-known empirical correlation given by eq. (7) [26,27], while A_S depends on the particle diameter (d_p, assumed to be 0.03 m) and void fraction (ε) as reported in eq. (8):

$$Nu=2.0+1.1\cdot Re_p{}^{0.6}\cdot Pr^{0.33} \quad (7)$$

$$A_S=\frac{6\cdot(1-\varepsilon)}{d_p} \quad (8)$$

The effective thermal conductivity, k_{eff}, of the bed, given by eq. (9), takes into account the conductivity of both the solid medium and the working fluid; it also includes the effects of thermal radiation, which are non-negligible at temperatures higher than 300 °C [28]:

$$k_{eff} = k_{WF}\left[\varepsilon\left(1+\tau\frac{\alpha_{rv}d_p}{k_{WF}}\right)+\frac{\tau(1-\varepsilon)}{\frac{1}{\frac{1}{\phi}+\frac{\alpha_{rs}d_p}{k_{WF}}}+\frac{\theta}{\kappa}}\right] \quad (9)$$

where k_S and k_{WF} represent the thermal conductivity of the solid medium and working fluid, respectively, while κ is their ratio, τ represents the ratio of the distance of the centres of two adjacent solid pebbles to the diameter of the pebble (set to 0.9), θ is the ratio of the pebble length affected by the thermal conductivity to the diameter of the pebble (set to 2/3), ϕ is a parameter that measures the thickness of the fluid film adjacent to the contact point of two solid pebbles that depends on the bed void, obtained according the correlations proposed in [25,28], and α_{rv} and α_{rs} are the void-to-void radiative heat transfer coefficient and solid-to-solid surface radiative heat transfer coefficient, respectively, calculated according to the following correlations:

$$\alpha_{rv} = \left[\frac{0.1952}{\left(1+\frac{\varepsilon}{2(1-\varepsilon)}\frac{1-\epsilon_s}{\epsilon_s}\right)}\right]\left(\frac{T_{WF}}{100}\right)^3 \quad (10)$$

$$\alpha_{rs} = 0.1952\left(\frac{\epsilon_s}{2-\epsilon_s}\right)\left(\frac{T_S}{100}\right)^3 \quad (11)$$

where ϵ_s is the solid emissivity (imposed to be 0.85). A spatial step of 0.05 m and a variable timestep with a maximum of 10 s were imposed during the simulation. To minimize the hysteresis effect, the temperature profiles obtained after five complete charging–discharging cycles are taken as references for the evaluation of the useful storage zone.

3.3. Performance indices

Several indices are defined and analysed to characterize the performance of the integrated PTES–CSP plant by varying the main design parameters, such as pressure ratio β_C and WCOs outlet temperature. All the performance indices refer to nominal conditions, with a constant mass flow rate of the working fluid regardless of the operating mode. Because the integrated system is fed by two energy sources characterized by a different energy quality, namely, the electrical energy from the grid and the thermal energy in the solar receiver, the performance is evaluated by analysing the exergy flows instead of the energetic ones.

The performance indices are evaluated by assuming that the integrated plant is completely fed by the TES system during the discharging phase, without the use of external energy sources. Moreover, the TES thermal losses are assumed negligible and maximum and minimum temperatures inside the three storage vessels are kept constant during the charging-discharging cycle

The first performance index is the nominal exergy roundtrip efficiency of the integrated PTES–CSP system ($\eta_{RT,PTES-CSP}$). It is defined as the ratio of the time integral of the nominal power delivered during the discharging phase ($\dot{W}_{PTES-CSP,D}$) to the time integral of the sum of the nominal absorbed electrical power ($\dot{W}_{PTES,C}$) and the nominal exergy input in the solar receiver ($\dot{E}_R$) during the charging phase:

$$\eta_{RT,PTES-CSP} = \frac{\int_0^{t_D} \dot{W}_{PTES-CSP,D} dt}{\int_0^{t_C} (|\dot{W}_{PTES,C}| + \dot{E}_R) dt} \quad (12)$$

where t_C and t_D are the nominal charging and discharging times, respectively.

According to the abovementioned assumptions, the exergy flows remain constant during the charging-discharging cycles, and, neglecting thermal losses, the discharging time (t_D) is equal to the charging time (t_C). Consequently, the nominal roundtrip efficiency of the integrated PTES–CSP system can be expressed as:

$$\eta_{RT,PTES-CSP} = \frac{\dot{W}_{PTES-CSP,D} \cdot t_D}{(|\dot{W}_{PTES,C}| + \dot{E}_R) \cdot t_C} = \frac{\dot{W}_{PTES-CSP,D}}{(|\dot{W}_{PTES,C}| + \dot{E}_R)} \quad (13)$$

Since the mass flow rate of the working fluid does not vary between the charging and the discharging phases, $\eta_{RT,PTES-CSP}$ can be simply expressed as the ratio between the specific product exergy during the discharging phase and the specific fuel exergy during the charging phase:

$$\eta_{RT,PTES-CSP} = \frac{(h_{4D} - h_{7D}) - (h_{3D} - h_{2D})}{(h_{2C} - h_{1C}) - (h_{6C} - h_{7C}) + (e_{3C} - e_{2C})} \quad (14)$$

A second performance index concerns the nominal roundtrip efficiency ($\eta_{RT,PTES}$) of the sole PTES section, which is defined as the ratio of the time integral of the electric power produced by the sole PTES section during the discharging phase ($\dot{W}_{PTES,D}$) to the time integral of the electric power absorbed during the charging phase ($\dot{W}_{PTES,C}$):

$$\eta_{RT,PTES} = \frac{\int_0^{t_D} \dot{W}_{PTES,D} dt}{\int_0^{t_C} |\dot{W}_{PTES,C}| dt} \quad (15)$$

Similarly to the previous index, $\eta_{RT,PTES}$ can be operatively expressed as:

$$\eta_{RT,PTES} = \frac{\dot{W}_{PTES,D} \cdot t_D}{|\dot{W}_{PTES,C}| \cdot t_C} = \frac{\dot{W}_{PTES,D}}{|\dot{W}_{PTES,C}|} = \frac{(h_{4D} - h_{7D}) - (h_{3D} - h_{2D})}{(h_{2C} - h_{1C}) - (h_{6C} - h_{7C})} \quad (16)$$

The exergy efficiency of the system when only the CSP section is in operation (η_{CSP}) is also investigated as a third performance index. It is defined as the ratio of the power produced by the CSP section in a stand-alone operation ($\dot{W}_{CSP}$) to the exergy input in the solar receiver ($\dot{E}_R$):

$$\eta_{CSP} = \frac{\dot{W}_{CSP}}{\dot{E}_R} = \frac{(h_{5D} - h_{6D}) - (h_{2C} - h_{1C})}{(e_{3C} - e_{2C})} \quad (17)$$

Finally, a PTES power share (γ) is introduced to investigate the weight of the PTES section compared to that of the overall PTES–CSP plant. The power share is the ratio of the nominal power produced by the PTES section ($\dot{W}_{PTES,D}$) to the nominal power produced by the integrated PTES–CSP system ($\dot{W}_{PTES-CSP,D}$) during the discharging phase:

$$\gamma = \frac{\dot{W}_{PTES,D}}{\dot{W}_{PTES-CSP,D}} = \frac{(h_{4D} - h_{7D}) - (h_{3D} - h_{2D})}{(h_{5D} - h_{6D}) - (h_{3D} - h_{2D})} \quad (18)$$

4. Results and discussion

In this section, the performance of the integrated PTES–CSP system under design conditions as a function of the different design parameters, namely, pressure ratio and outlet temperatures of the water coolers (that is, the temperature imposed in section 6C of Figure 3 and section 1D of Figure 4), is presented and discussed. Figure 7(a–d) shows the performance indices defined in the previous section as a function of the pressure ratio (β_C), by assuming a maximum temperature at the outlet of the solar receiver of 1000 K and optimized WCO1 and WCO2/WCO3 outlet temperatures. The optimization process was carried out by finding the temperatures that allow maximization of the roundtrip efficiency of the integrated PTES–CSP plant for a given pressure ratio. As shown in Figure 7(a), an increase of β_C leads to an initial improvement of the system performance both in the case of operating in integrated mode and in PTES-only mode. In fact, the reduction of the heat released to the environment by WCO2 and WCO3 achieved with the rise in pressure ratio leads to an improvement of the performance during the discharging phase. As can be observed in Figure 7(b), the rise in the pressure ratio also leads to a decrease of the optimal WCO2 outlet temperature, which also defines the maximum temperature in the MT-TES and the inlet temperature in the solar receiver, while the optimal outlet temperature of the WCO1 remains constant and equal to the imposed minimum one. It is worth noting that the optimal WCO2 outlet temperature coincides with the maximum temperature that satisfies the turbomachinery maximum temperature constraint. An increase of this threshold would therefore lead to an increase of the optimal WCO2 outlet temperature and a consequent enhancement of the system performance. The roundtrip efficiency increases with the rise of β_C until a maximum value is reached for a value of β_C of about 5.2. In these conditions, the constraint related to the minimum temperature achievable in the turbomachinery becomes stricter and a further rise in β_C requires an appropriate rise in the WCO1 outlet temperature to keep a minimum cycle temperature higher than 173 K. Consequently, starting from this condition, the benefits to system performance during the discharging phase deriving from the rise of the pressure ratio are compensated by the significant increase of heat released by WCO1, with the subsequent decrement of performance during the charging phase.

As shown by Figure 7(c), the exergy efficiency achieved when only the CSP section is in operation is negative for pressure ratios lower than 3.8, and even for the highest β_C value the efficiency is below 0.15.

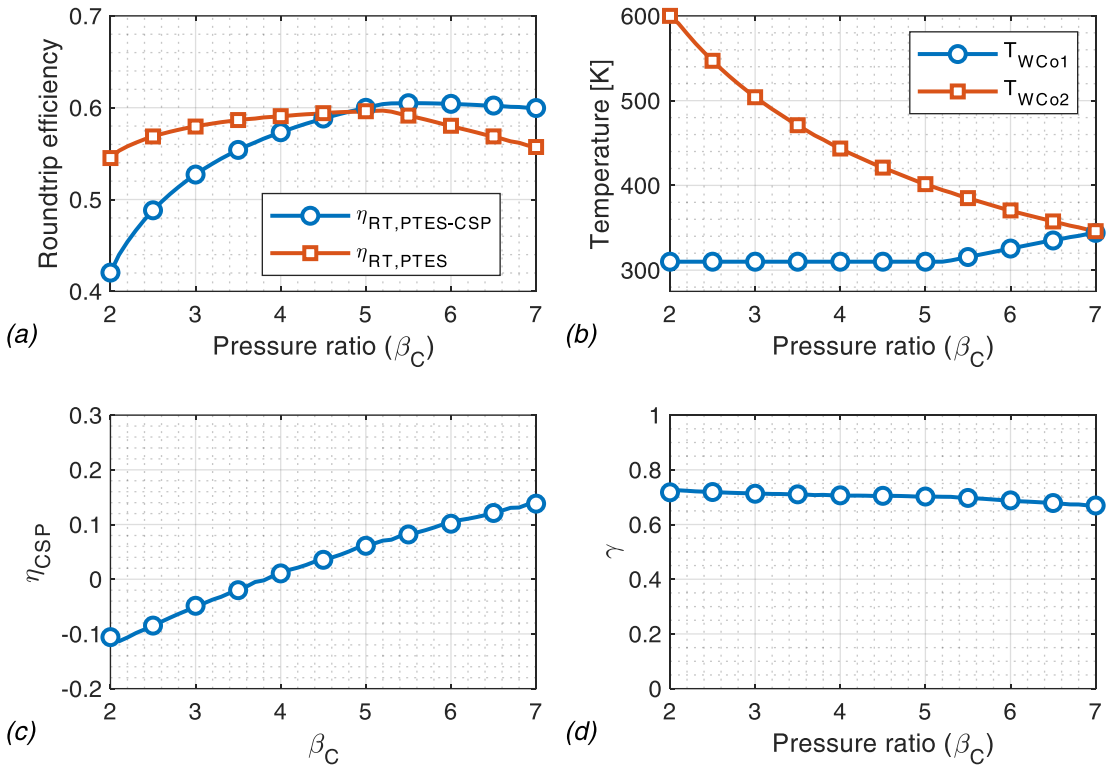

Figure 7 – Maximum performance indices achieved by the integrated PTES–CSP plant as a function of the compressor pressure ratio by assuming a maximum temperature of 1000 K.

In fact, the design of the system is based on optimizing the performance of the integrated PTES–CSP plant and the operability of the sole CSP section is assumed as infrequent. Enhancement of this performance parameter could be achieved by reducing the WCO2 outlet temperature. However, this design choice would also affect the performance of the PTES section, with an overall degradation of the integrated PTES–CSP plant's performance.

Finally, the variation of the PTES power share shown in Figure 7(d) is rather limited in the assumed variation range of β_C (values of γ are around 0.7). A significant change in the weight of the two power outputs is therefore achievable only with an increase of the maximum temperature in the solar receiver or with a decrease of the WCO2 design outlet temperature (with the consequent decrease of roundtrip efficiency).

4.1. Plant sizing

The results previously discussed demonstrate that maximization of the PTES–CSP roundtrip efficiency is achieved by increasing the pressure ratio until the WCO2 outlet temperature remains at its lowest value and with a WCO1 outlet temperature chosen to reach the maximum allowable temperature on the compressor outlet side. Following this design approach, the thermodynamic cycles of the various operating modes are therefore defined. As mentioned in the previous section, sizing of the various components requires the definition of two other design parameters, namely, the net power produced by the integrated PTES–CSP plant and the nominal storage capacity of the three storage tanks. In this study, sizing of the plant was carried out by setting a nominal

net power of 5 MW and a storage capacity of 4 equivalent hours of plant operation at nominal conditions. The most important results of the preliminary design of the integrated PTES–CSP plant are reported in Table 2.

Table 2 – Preliminary design of the integrated PTES–CSP plant.

Design parameters		**Component size**	
Pressure ratio	5.2	Mass flow rate	38.6 kg/s
WCO1 outlet temperature	310 K	Compressor C1 nominal power	8.61 MW
WCO2 outlet temperature	395 K	Compressor C2 nominal power	3.77 MW
PTES–CSP net power	5 MW	Turbine T1 nominal power	2.73 MW
TES capacity	4 hours	Turbine T2 nominal power	7.28 MW
Performance indices		Turbine T3 nominal power	8.77 MW
PTES–CSP roundtrip efficiency ($\eta_{RT,PTES-CSP}$)	60.4%	Solar receiver thermal input	3.58 MW_t
PTES-only roundtrip efficiency ($\eta_{RT,PTES}$)	59.7%	WCO1 nominal heat released	1.05 MW_t
CSP-only efficiency (η_{CSP})	7.1%	WCO2 nominal heat released	1.32 MW_t
PTES power share (γ)	70.0%	WCO3 nominal heat released	3.40 MW_t

Table 3 reports a preliminary design for the three storage tanks, including the storage volume required in terms of theoretical ($V_{TES,t}$) and actual vessel volume ($V_{TES,r}$) and the corresponding diameter and height (an aspect ratio of 3 was assumed). Although the difference between the maximum and minimum temperature of the working fluid along the bed is at a maximum for the MT-TES, the required theoretical volume for this tank is smaller than that of the LT-TES one. This is due to the strong increase of the specific heat of the granite pebbles with temperature as shown in Figure 6, with a corresponding decrease of the required storage volume per unit of temperature variation.

As already mentioned, the need to keep fixed temperatures at the inlet and outlet sides of the packed bed results from the presence of a thermocline inside the tank at the end of each cycle. This leads to a strong increase in the actual storage volume required by the three TES systems. In particular, an increment of about ten times the theoretical storage volume occurs if no thresholds in the outlet temperature are imposed, that is no tolerances in the minimum and maximum temperatures are allowed during the charging and discharging phases. To avoid the requirement for vessels with a very large storage volume, with a consequent rise in the capital costs, a tolerance in outlet temperature of 20 K is therefore assumed, resulting in a reduction in the actual TES volume of more than 60% compared to the no-threshold case. Consequently, as reported in Table 3, the actual storage volume required by the three TES systems is about three times the minimum theoretical storage volume. The largest increase is observed for the MT-TES, since it is characterized by the highest temperature difference and the consequent decrement of the useful storage zone. Because the hysteresis effect reduces the useful storage zone with the progression of the cycles, the temperature profiles obtained after five complete charging–discharging cycles are used. By way of example, Figure 8 shows the temperature profiles within the LT-TES and MT-TES obtained at the end of the charging and discharging phases in the fifth cycle. The figure highlights

the useful storage zone as the area enclosed between the two temperature profiles as well as the variation in the minimum and maximum temperatures achieved at the end of the charging and discharging phases due to the introduction of a temperature threshold of 20 K.

Table 3 – Main design parameters for the three TES systems of the proposed PTES–CSP plant.

Storage system		**LT-TES**	**MT-TES**	**HT-TES**
Temperature difference [K]		224	458	181
Theoretical TES volume ($V_{TES,t}$) [m^3]		254	191	172
Actual TES volume ($V_{TES,r}$) [m^3]	*No threshold*	2032	2032	1452
	With threshold (20 K)	782	782	452
Diameter [m]		14.4	14.4	12.0
Height [m]		4.8	4.8	4.0

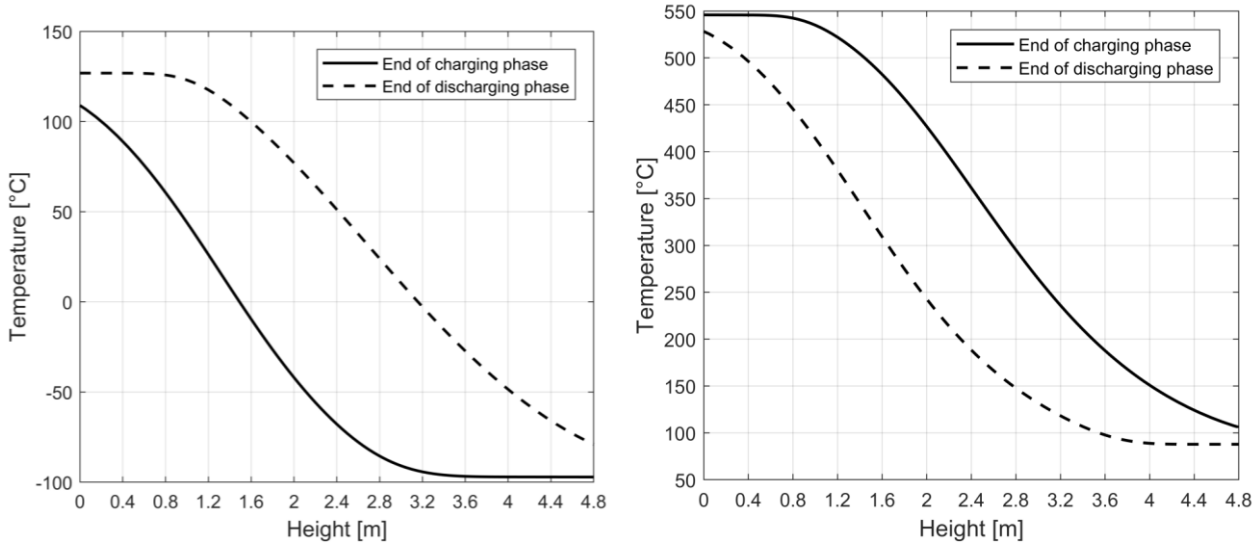

Figure 8 – Temperature profiles of the LT-TES (left side) and MT-TES (right side) at the end of the charging and discharging phases with an outlet temperature threshold of 20 K.

4.2. Outlet receiver temperature effect

In the previous analysis, the maximum temperature achieved in the solar receiver (T_{3C}) was assumed to be constant and equal to 1000 K. Depending on both the receiver design and the concentrating factor imposed for the solar field, different temperatures could be obtained. Therefore, the effect of this design parameter on the main plant performance indices was investigated and the main results are shown in *Figure 9*. It is worth noting that the performance of the PTES section is not affected by this design parameter (no changes in the minimum and maximum temperatures occur in the LT-TES and MT-TES) or by the optimal outlet temperature of the water coolers. On the other hand, the conversion efficiency of the CSP plant as well as its weight in the overall net power output vary widely with this parameter. As shown in *Figure 9*(a), an increase of 50 K could lead to

an increase of the CSP-only efficiency of more than 10 percentage points, regardless of the imposed pressure ratio. It is therefore clear that an integrated PTES–CSP plant designed for large use of the CSP-only operating mode requires the achievement of high temperatures in the receiver although the benefits in performance will become more and more marginal with a rise in T_{3C}. As shown in *Figure 9*(b), a decrease of about 5 percentage points in the power ratio index occurs with a 50 K rise in the maximum temperature. These variations are then reflected in the trend of the roundtrip efficiency of the integrated PTES–CSP plant, as shown in *Figure 9*(c). A rise in the outlet receiver temperature and a simultaneous increase of the weight of the CSP plant, characterized by a lower conversion efficiency, are not beneficial for lower pressure ratios but the performance increment of the solar section with the rise of β_C leads to a turnaround and the benefits of increasing the maximum temperature become visible for $\beta_C > 5$. Furthermore, an increase in the optimal pressure ratio (previously detected as 5.2) is also observed, despite the decline in performance in the PTES section.

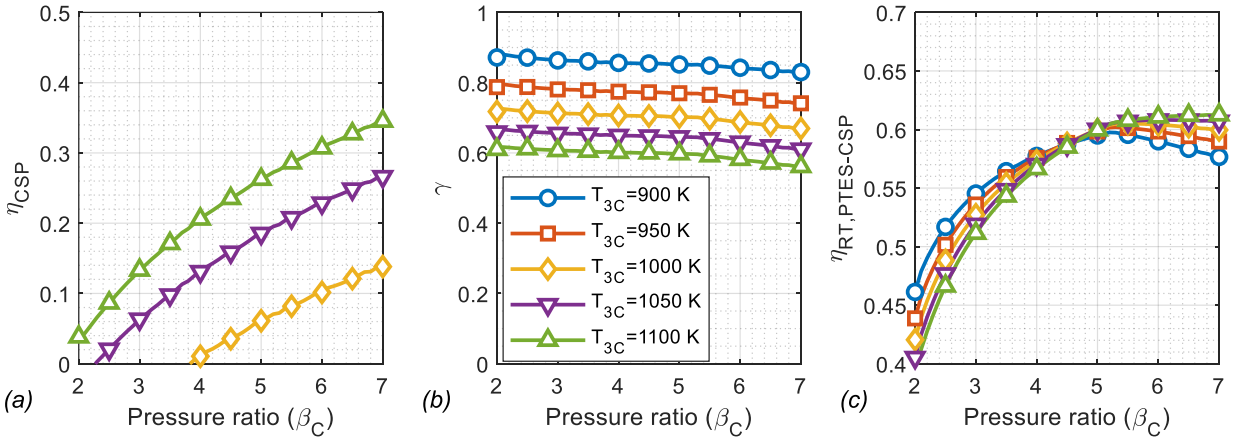

Figure 9 – Main performance indices achieved by the integrated PTES–CSP plant as a function of the maximum cycle temperature.

4.3. Turbomachinery performance effect

The performance of the integrated PTES–CSP plant is also strongly influenced by the technology level of compressors and turbines. In particular, two main turbomachinery parameters influence the performance of the plant under nominal conditions: the polytropic efficiency and the maximum operating temperatures. Figure 10(a–d) shows the variation of the main performance indices with the polytropic efficiency by varying the pressure ratio. The polytropic efficiency is explanatory of the technology level of turbomachines and no difference among compressors and expanders is introduced ($\eta_C = \eta_T$). As shown in Figure 10(a), the turbomachinery efficiency strongly influences the PTES roundtrip efficiency, with an increment of about 3 percentage points per percentage point of increment in the polytropic efficiency. This behaviour, already shown by other published papers [10,12], highlights the need for compressors and expanders with a high technology level if competitive roundtrip efficiencies are to be achieved. Also, the efficiency of the CSP plant in stand-alone operating mode (Figure 10(b)) could largely benefit from an increase of the compressor/turbine polytropic efficiency while this operating mode is not allowable for efficiency values lower than 0.90. These trends are obviously reflected in the roundtrip efficiency of the integrated plant, as shown in Figure 10(c),

especially for plant designs characterized by high pressure ratios while, as shown by Figure 10(d), the power ratio between the two section remains almost constant.

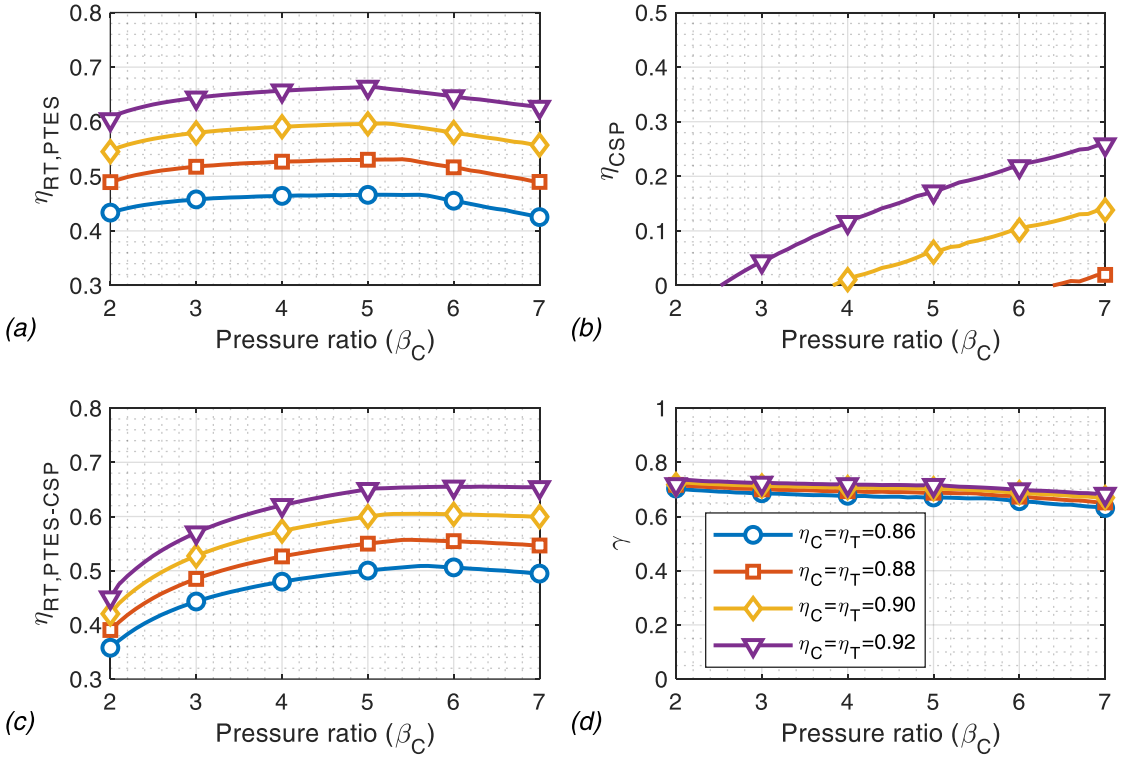

Figure 10 – Main performance indices achieved by the integrated PTES–CSP plant as a function of turbomachinery polytropic efficiency.

The temperature limits imposed for compressors and turbines also strongly affect the performance of the integrated system since they correspond to the minimum and maximum allowed temperature in the PTES section. As demonstrated by the previous results, for a given pressure ratio the optimal WCO2 temperature was determined to keep an outlet C1 temperature equal to the maximum allowed, while the best performance was achieved for the lowest value of pressure ratio that assures the minimum allowable temperature at the outlet side of the turbine T1. Therefore, it is evident that a relaxation in the temperature bounds will result in an enhancement of the PTES performance. By way of example, Figure 11(a–d) shows the impact of the maximum allowable temperature (T_{MAX}) in the compressors/turbines on the main performance indices.

As expected, a rise in the maximum allowable temperature, and thus in the maximum temperature of the Brayton cycle followed by the PTES section, leads to an improvement of the roundtrip efficiency during PTES-only operation (Figure 11(a)). Simultaneously, as can be observed in Figure 11(b), a strong drop in η_{CSP} and the consequent impossibility of following CSP-only operation occur since an increase of the outlet temperature C1 leads to negative efficiencies regardless of the compressor pressure ratio imposed.

However, this drawback is not reflected in the roundtrip efficiency of the integrated plant (Figure 11(c)) since, as shown in Figure 11(d), the weight of the CSP plant becomes more and more marginal with a rise of the maximum allowable temperature and γ approaches unity for pressure ratios higher than 3. In these conditions,

the benefits of integrating the PTES system with a solar section will become insignificant without a rise in the maximum receiver temperature.

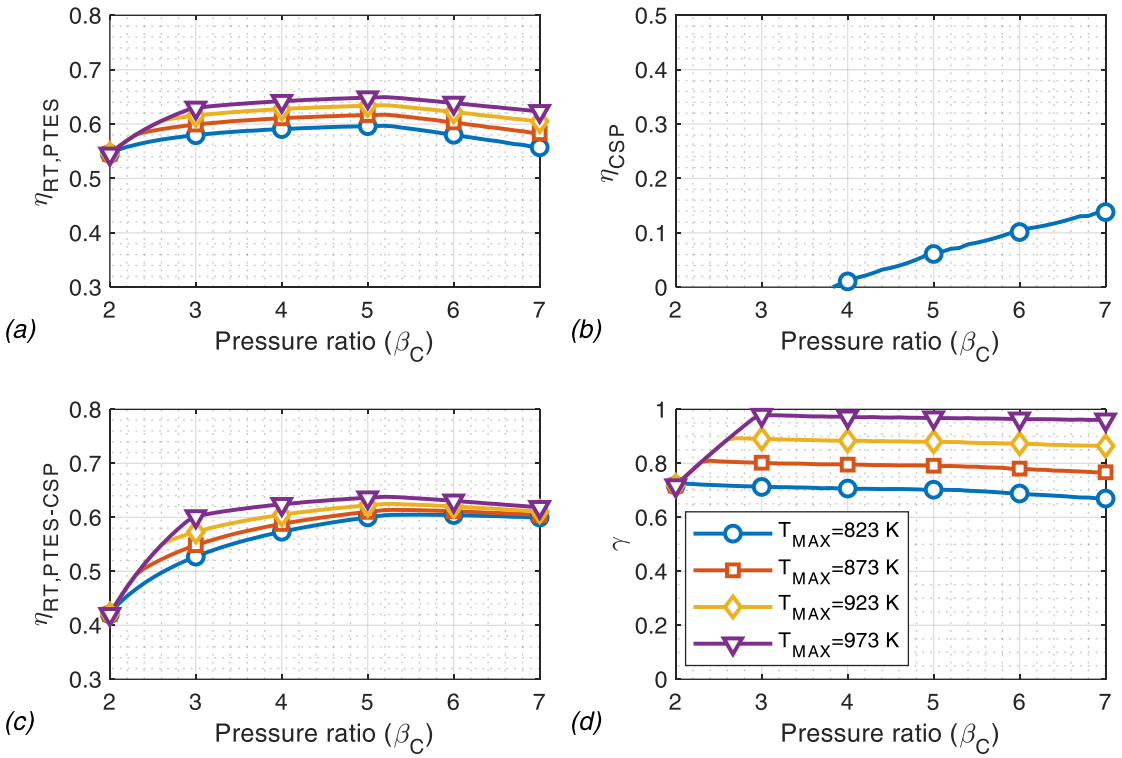

Figure 11 – Main performance indices achieved by the integrated PTES–CSP plant as a function of turbomachinery maximum temperature.

5. Conclusions

An innovative PTES system integrated with a CSP plant based on a closed-loop Brayton-Joule cycle was proposed and analysed in this study. The integrated PTES–CSP plant includes three TES storage tanks and argon was chosen as the working fluid. Specific mathematical models were developed to simulate the PTES and CSP sections under design conditions, as well as to calculate the thermal behaviour of the different TES storage tanks during the charging and discharging processes and to assess the required storage volumes.

The study demonstrated that maximization of the PTES–CSP exergetic roundtrip efficiency is achieved by increasing the pressure ratio until the maximum temperature of the LT-TES remains at its lowest value. Furthermore, the outlet temperature of the water cooler downstream of the MT-TES should be chosen to reach the maximum allowable temperature at the compressor outlet side. The plant's performance is strongly influenced by the turbomachinery technology level. A rise in the expected polytropic efficiency and the ability to operate in a wider temperature range would result in a significant performance enhancement, achieving roundtrip efficiencies comparable with those of PHES systems. The influence of the maximum temperature achieved in the solar receiver on the main plant performance indices was also investigated, highlighting a shift of the optimal pressure ratio toward higher values and the consequent performance improvement, especially in the CSP section with a rise of this design parameter.

A feasible design for the PTES–CSP system with a rated power of 5 MW and 4 hours of storage capacity was then proposed, achieving an exergetic roundtrip efficiency of the integrated plant of about 60%. On the other hand, since all the plant components should frequently operate far from their nominal conditions (due to fluctuation in both storage service requirements and solar energy availability), the actual capabilities of the integrated system during the operating phases should be investigated. For this reason, the development of specific mathematical models for investigating the plant's performance under off-design conditions, as well as the study of suitable control strategies for optimum management of the integrated plant, are currently under development for future works.

Acknowledgments

This paper is also part of the research project funded by P.O.R. SARDEGNA F.S.E. 2014-2020 – Axis III Education and Training, Thematic Goal 10, Specific Goal 10.5, Action Partnership Agreement 10.5.12 – "Call for funding of research projects – Year 2017".

References

[1] Guerrero J, Blaabjerg F, Zhelev T, Hemmes K, Monmasson E, Jemei S, et al. Distributed Generation: Toward a New Energy Paradigm. IEEE Ind Electron Mag 2010;4:52–64. doi:10.1109/MIE.2010.935862.

[2] Aneke M, Wang M. Energy storage technologies and real life applications – A state of the art review. Appl Energy 2016;179:350–77. doi:10.1016/j.apenergy.2016.06.097.

[3] Yekini Suberu M, Wazir Mustafa M, Bashir N. Energy storage systems for renewable energy power sector integration and mitigation of intermittency. Renew Sustain Energy Rev 2014;35:499–514. doi:10.1016/j.rser.2014.04.009.

[4] Budt M, Wolf D, Span R, Yan J. A review on compressed air energy storage: Basic principles, past milestones and recent developments. Appl Energy 2016;170:250–68. doi:10.1016/j.apenergy.2016.02.108.

[5] Frate GF, Ferrari L, Desideri U. Energy storage for grid-scale applications: Technology review and economic feasibility analysis. Renew Energy 2021;163:1754–72. doi:10.1016/j.renene.2020.10.070.

[6] Frate GF, Ferrari L, Desideri U. Multi-criteria investigation of a pumped thermal electricity storage (PTES) system with thermal integration and sensible heat storage. Energy Convers Manag 2020;208:112530. doi:10.1016/j.enconman.2020.112530.

[7] White A, Parks G, Markides CN. Thermodynamic analysis of pumped thermal electricity storage. Appl Therm Eng 2013;53:291–8. doi:10.1016/j.applthermaleng.2012.03.030.

[8] Benato A, Stoppato A. Pumped Thermal Electricity Storage: A technology overview. Therm Sci Eng Prog 2018;6:301–15. doi:10.1016/j.tsep.2018.01.017.

[9] Guo J, Cai L, Chen J, Zhou Y. Performance evaluation and parametric choice criteria of a Brayton pumped thermal electricity storage system. Energy 2016;113:693–701.

doi:10.1016/j.energy.2016.07.080.

[10] McTigue JD, White AJ, Markides CN. Parametric studies and optimisation of pumped thermal electricity storage. Appl Energy 2015;137:800–11. doi:10.1016/j.apenergy.2014.08.039.

[11] Zhao Y, Liu M, Song J, Wang C, Yan J, Markides CN. Advanced exergy analysis of a Joule-Brayton pumped thermal electricity storage system with liquid-phase storage. Energy Convers Manag 2021;231:113867. doi:10.1016/J.ENCONMAN.2021.113867.

[12] Wang L, Lin X, Chai L, Peng L, Yu D, Chen H. Cyclic transient behavior of the Joule–Brayton based pumped heat electricity storage: Modeling and analysis. Renew Sustain Energy Rev 2019;111:523–34. doi:10.1016/j.rser.2019.03.056.

[13] Wang L, Lin X, Zhang H, Peng L, Chen H. Brayton-cycle-based pumped heat electricity storage with innovative operation mode of thermal energy storage array. Appl Energy 2021;291:116821. doi:10.1016/j.apenergy.2021.116821.

[14] Benato A, Stoppato A. Heat transfer fluid and material selection for an innovative Pumped Thermal Electricity Storage system. Energy 2018;147:155–68. doi:10.1016/j.energy.2018.01.045.

[15] Dumont O, Frate GF, Pillai A, Lecompte S, De paepe M, Lemort V. Carnot battery technology: A state-of-the-art review. J Energy Storage 2020;32:101756. doi:10.1016/j.est.2020.101756.

[16] Benato A. Performance and cost evaluation of an innovative Pumped Thermal Electricity Storage power system. Energy 2017;138:419–36. doi:10.1016/j.energy.2017.07.066.

[17] Zhang H, Wang L, Lin X, Chen H. Combined cooling, heating, and power generation performance of pumped thermal electricity storage system based on Brayton cycle. Appl Energy 2020;278:115607. doi:10.1016/j.apenergy.2020.115607.

[18] Jockenhöfer H, Steinmann WD, Bauer D. Detailed numerical investigation of a pumped thermal energy storage with low temperature heat integration. Energy 2018;145:665–76. doi:10.1016/j.energy.2017.12.087.

[19] Wang G-B, Zhang X-R. Thermodynamic analysis of a novel pumped thermal energy storage system utilizing ambient thermal energy and LNG cold energy. Energy Convers Manag 2017;148:1248–64. doi:10.1016/j.enconman.2017.06.044.

[20] Augustine C, Turchi C, Mehos M. The Role of Concentrating Solar-Thermal Technologies in a Decarbonized U.S. Grid. Natl Renew Energy Lab 2021.

[21] McTigue J, Farres-Antunez P, Ellingwood K, Neises T, White A. Pumped thermal electricity storage with supercritical CO2 cycles and solar heat input. AIP Conf. Proc., vol. 2303, AIP Publishing; 2020, p. 190024. doi:10.1063/5.0032337.

[22] Sedighi M, Padilla RV, Taylor RA, Lake M, Izadgoshasb I, Rose A. High-temperature, point-focus, pressurised gas-phase solar receivers: A comprehensive review. Energy Convers Manag 2019;185:678–717. doi:10.1016/J.ENCONMAN.2019.02.020.

[23] Chai L, Liu J, Wang L, Yue L, Yang L, Sheng Y, et al. Cryogenic energy storage characteristics of a packed bed at different pressures. Appl Therm Eng 2014;63:439–46.

doi:10.1016/j.applthermaleng.2013.11.030.

[24] Heuze FE. High-temperature mechanical, physical and Thermal properties of granitic rocks— A review. Int J Rock Mech Min Sci Geomech Abstr 1983;20:3–10. doi:10.1016/0148-9062(83)91609-1.

[25] Zanganeh G, Pedretti A, Zavattoni S, Barbato M, Steinfeld A. Packed-bed thermal storage for concentrated solar power - Pilot-scale demonstration and industrial-scale design. Sol Energy 2012;86:3084–98. doi:10.1016/j.solener.2012.07.019.

[26] Cascetta M, Serra F, Arena S, Casti E, Cau G, Puddu P. Experimental and Numerical Research Activity on a Packed Bed TES System. Energies 2016;9:758. doi:10.3390/en9090758.

[27] Wakao, N., Kaguei S. Heat and Mass Transfer in Packed Beds. New York: 1982.

[28] Kunii D, Smith JM. Heat transfer characteristics of porous rocks. AIChE J 1960;6:71–8. doi:10.1002/aic.690060115.